## ORIGINAL RESEARCH PAPER

# Nano LTA Zeolite in Water Softening Process: Synthesis, Characterization, Kinetic studies and process optimization by Response Surface Methodology (RSM)

**Elmira Ghadamnan[1], Seyed Reza Nabavi[1,]\*, Mahmoud Abbasi[2]**

[1] *Department of Applied Chemistry, University of Mazandaran, Babolsar, Iran*
[2] *Applied Electrochemistry, School of Chemical Science and Engineering, KTH Royal Institute of Technology, Teknikringen 42, SE-100 44 Stockholm, Sweden*

**ABSTRACT**

In the present study, nano zeolite A (LTA) was synthesized by the alkaline fusion method without adding an organic template. Effect of temperature and aging time were studied on the crystallinity and morphology of the final product. The synthesized LTA was characterized by scanning electron microscopy (SEM), energy dispersive X-ray spectroscopy (EDX), powder X-ray diffraction (XRD), Fourier transform infrared spectroscopy (FTIR), thermal gravimetric analysis (TGA), differential scanning calorimetry (DSC) and $N_2$ adsorption/desorption technique. The prepared nano LTA zeolite was applied to the water softening process. The main effects and interaction of factors such as pH, the amount of LTA, initial total hardness, temperature and contact time were investigated by response surface methodology (RSM). The obtained optimum values of factors were applied to hard water to remove $Ca^{2+}$ and $Mg^{2+}$ ions. Pseudo-first and second-order models were applied to kinetic and rate data. It was found that the adsorption rate follows the pseudo-second-order kinetic model.

**Keywords:** *Nano LTA zeolite; Alkaline fusion method, Water softening; Water Hardness; Adsorption; RSM*

## INTRODUCTION

The hardness in water mostly represents the contents of calcium and magnesium. It ascribed the total concentration of calcium and magnesium and declared in terms of the calcium carbonate equivalent. In the standard scale, soft, moderate, hard and very hard water contains about 0–60, 61–120, 121–180 and >180 mgL$^{-1}$ of $Ca^{2+}$ or $Mg^{2+}$, respectively [1]. More than three-quarters of the water supplies are so hard water that would easily be deposited in the form of scale on the surfaces of equipment like pipes, cooling and heating systems, steam generation, bathtubs, kitchen appliances, and undesirable spots on sinks and clothes. The formation of scale causes clogging of a piping system and boilers thus lowering the water flow as well as corrosion surfaces and shortened operational life of the equipment [2, 3].

Nevertheless, both calcium and magnesium are essential minerals and advantageous to human health, but their excess causes health problems. The health problems such as dermatitis, diarrheal-disease, pancreatic cancer, cardiovascular disease, cerebrovascular mortality, malformations of the central nervous system, Alzheimer's disease, diabetes, childhood atopic dermatitis, kidney stones, reproductive health, digestive health and constipation, and bone mineral density can be counted [4-6]. Water softening can be regarded as a treatment process where the calcium and

\* Corresponding Author Email: *srnabavi@umz.ac.ir*

magnesium cations are removed from the water.

Several methods have been recommended in literature to treat the problems induced hard water. These methods can be listed as chemical precipitation [7], adsorption and ion exchange [8], micro and nanofiltration [9], electrodeionization [10], reverse osmosis (RO) [11] and finally membrane-based technologies [12]. Among the former methods, ion exchange and adsorption processes by zeolites are more practical due to their remarkable advantages like low cost, simplicity and high selectivity [13-15].

Zeolites occur both naturally and synthetic forms. In brief, these materials are porous crystalline aluminosilicates with a three-dimensional network of $SiO_4^{4-}$ and $AlO_4^{5-}$ tetrahedral units linked by oxygen bridges. Their framework structures contain channels and cavities occupied by the cations and water molecules [16, 17].

Zeolite A, LTA (Linde Type A) or 4A has a cubic structure with ($Na_{12}Al_{12}Si_{12}O_{48}$) formula and an aperture of $4\times4$ A˚, a low silica zeolite with Si/Al = 1 [18]. LTA framework type can be constructed with connecting sodalite cages (6-ring) via double 4-rings. Accordingly, it creates an alpha cavity (8-ring) in the unit cell center. The unit cell has 12 sodium cations per alpha cavity so that eight cations are considered in the eight 6-rings, and the four cations are located in the three 8-ring windows. It should be noted that one of the 8-membered rings is occupied using two sodium cations. Therefore it is more favorable to exchange with heavy metals. In the ion exchange process, two $Na^+$ cations can be substituted by one $Ca^{2+}$ cation [19]. LTA has a strong affinity for many heavy metal cations [20], and its cation exchange properties are commercially exploited in water softening to trap $Ca^{2+}$ and $Mg^{2+}$ cations [14, 21-23].

There are several reports for the synthesis of LTA with different starting materials like fly ash [24-26], Kaolin [27, 28] and scoria [29] using alkaline fusion procedure. Although the preparation of LTA from inexpensive starting materials is preferred, the synthesis of LTA from silica and alumina has the benefit of producing products with high purity and high surface area.

In the current study, nano LTA zeolite was synthesized from pure silica and alumina by the alkaline fusion followed by hydrothermal crystallization and without adding an organic template. Effects of temperature and aging time were studied on the crystallinity and morphology of the final product. The prepared nano LTA zeolite was then applied in the water softening process.

Since $Ca^{2+}$ and $Mg^{2+}$ ions exist simultaneously in nature and the total hardness consists of the sum of these two ions, therefore, the reduction of hardness requires reducing the concentration of both ions together. Most of the previous studies have been conducted to remove $Ca^{2+}$ and $Mg^{2+}$ ions in the single system [30, 31]. However, in the present study, the ion exchange process investigated in the binary system containing $Ca^{2+}$ and $Mg^{2+}$ ions using synthesized nano LTA zeolite. In order to find the optimum conditions of the water softening process, the main effects and interaction of factors such as pH, the amount of adsorbent, initial total hardness, temperature and contact time were evaluated by response surface methodology (RSM). The obtained optimum values of factors were applied to hard water in order to remove $Ca^{2+}$ and $Mg^{2+}$ simultaneously. In addition to, separation factor of adsorbent, competitive effects of ions and kinetics of ion exchange were investigated.

## EXPERIMENTAL

### Materials

Silica ($SiO_2$) powder (particles size $\approx$ 12 nm), alumina ($Al_2O_3$) powder and Sodium hydroxide (NaOH) as pellets (99%) were purchased from Sigma and Fluka respectively. calcium chloride and magnesium chloride in the analytical grade were bought from Merck, Germany. Ultra-pure deionized water was supplied from Zolalan Sharif (Iran) apparatus equipped with a double reverse osmosis unit.

### Characterization apparatuses

Surface morphology and the particles size of nano LTA zeolite were determined by a scanning electron microscope (SEM: KYKY-EM3200, 68 Hitachi Company, China) operating at 40 kx. X-ray diffraction (XRD, Philips, PW1730, Eindhoven, Netherland) technique was used to study the crystallinity. The IR bands of the synthesized zeolite were detected using the Fourier Transform Infrared (FTIR, Vector 22 Bruker, Germany) using a KBr wafer with the wave number ranging 400–4000 cm$^{-1}$. The specific surface area, pore volume, and pore size distribution were measured by the nitrogen adsorption-desorption method using the Brunauer-Emmett-Teller (BET) model and t-plot. All data were recorded and analyzed with BELsorp, Japan. Thermal gravimetric analysis (TGA) and differential scanning calorimetry (DSC) was performed with SETARAM, France.

120

*J. Water Environ. Nanotechnol., 4(2): 119-138 Spring 2019*

Magnesium ion concentration was obtained from atomic absorption spectrometry, PG-990, China. However, atomic emission spectrometry (PFP7, UK) was used to measure calcium ion concentration. The pH values of the solutions were adjusted from 2.0–10.0 adding either HCl and NaOH solution by pH-meter (Knick Elektronische Messgerate, Germany). In all ion exchange experiments, the temperatures of the solutions were controlled using a circulating bath (Julabo, Germany).

*Synthesis of nano LTA zeolite*

Sodium silicate ($Na_2SiO_4$) and sodium aluminate ($Na_2Al_2O_4$) were prepared by the alkaline fusion approach. In this procedure, 1.5 g of the $SiO_2$ powder was mixed with sodium hydroxide ($SiO_2$: NaOH = 1:1.2 in weight ratio) and then, to acquire the fused mass, the resultant mixture was fused at 750 $^o$C for 1 hour. A Similar method was performed to prepare sodium aluminate. In brief, 2.5 g of $Al_2O_3$ was mixed with NaOH ($Al_2O_3$: NaOH = 1:1.2 in weight ratio) and then was followed the resultant mixture fused at 450 $^o$C for 45 minutes.

To prepare sodium silicate and sodium aluminate solutions, first, the fused products were dissolved in deionized water and then, the clear supernatant achieved by filtering of the suspension to remove all un-reacted substrates.

In the next step, sodium aluminate solution was added into the sodium silicate solution drop by drop under vigorous stirring for two hours at room temperature. Accordingly, the non-crystalline aluminosilicate gel was synthesized. The crystallization process was performed using hydrothermal treatment as the growth of the crystals. The precursor gel was aged in an oven for 30, 48 and 72 hours at different temperature (i.e., 70, 90, 98 $^o$C) to achieve pure and single crystals phase, with uniform particle size. After the desired aging time and temperature, the obtained zeolite was filtered-off and rinsed with deionized water several times to remove excess alkali until the pH of the filtrate reached around 8. At the end of the process, the final synthesis product dried at 60 °C to eliminate the water extra blocked in the zeolite pores overnight and the obtained white powder was stored for characterization and application studies.

*The design of experiments*

RSM is the most popular method used in modeling and optimizing processes that the physical relationships between process decision factors have not been identified [32]. The central composite design (CCD) is one of the classes of RMS that extended from the full (or fractional) factorial design that offers a suitable model for curvature surface and considering the interaction of decision variables. The goal of CCD is to reduce experimental runs and investigate the main effect of each variable or their interactions [33, 34].

In the present study, the CCD was designed based on carrying out 16 factorial points (1/2 fraction of full factorial) 10 axial points, and three replicates at the center (total 29 experiments). In Table 1, the coded and uncoded values of the factors are shown. The Alpha value was calculated to equal to 2, according to $\alpha = \sqrt[4]{N_c}$ which makes design matrix rotatable. In this equation, $N_c$ defines the number of experiments considered in the fractional factorial design. Table 2 shows the details of the design

Table 1. Main parameters and their levels used in CCD.

| Parameters | Unit | Levels | | | | |
|---|---|---|---|---|---|---|
| Coded values | | -2 | -1 | · | +1 | +2 |
| $x_1$:pH | - | 2 | 4 | 6 | 8 | 10 |
| $x_2$:adsorbent amount | g | 0.02 | 0.05 | 0.08 | 0.11 | 0.14 |
| $x_3$:concentration cations | mgL$^{-1}$ | 150 | 200 | 250 | 300 | 350 |
| $x_4$:temperature | $^0$C | 11 | 17 | 23 | 29 | 35 |
| $x_5$: contact time | min | 15 | 40 | 65 | 90 | 115 |

Table 2. The pore structure properties of nano LTA that were calculated from BET model and t-plots.

| | | |
|---|---|---|
| BET | Total specific surface area ($S_{BET}$, m$^2$ g$^{-1}$) | 352.52 |
| | Micropore volume ($V_p$, cm$^3$ g$^{-1}$) | 0.14 |
| t-plot | Total specific surface area ($a_1$, m$^2$ g$^{-1}$) | 351.77 |
| | External specific surface area ($a_2$, m$^2$ g$^{-1}$) | 0.81 |
| | Micropore area ($a_1$- $a_2$, m$^2$ g$^{-1}$) | 350.95 |
| | Micropore volume ($V_p$, cm$^3$ g$^{-1}$) | 0.14 |
| | Micropore width (2t) (nm) | 0.82 |

*J. Water Environ. Nanotechnol., 4(2): 119-138 Spring 2019*

121

matrix and the response of each trial measured and predicted by the model. The full quadratic model was used to represent the influence of each factor on the response as follows Eq. (1).

$$y = a_0 + \sum_{i=1}^{4} a_i x_i + \sum_{i=1}^{4} a_{ii} x_i^2 + \sum_{i=1}^{4} \sum_{i \neq j, j=1}^{4} a_{ij} x_i x_j \qquad (1)$$

where, $y$ is the predicted response; $a_0$, $a_i$, $a_{ii}$ and $a_{ij}$ are the regression coefficients for the offset, linear, quadratic and interaction coefficients, respectively; $x_i$ and $x_j$ are the coded values of factors [35, 36]

The analysis of variance (ANOVA) was performed to justify the significance and adequacy of the developed model at 5% level of significance ($p = 0.05$). The quality of the regression model was evaluated by testing it for the lack of fit. The goodness of fitting was assessed by calculating the determination coefficient ($R^2$).

*Batch adsorption studies by CCD*

CCD with five decision variables was applied to optimize the ion exchange process. In the current study, these factors and the corresponding lower and upper limits were given in Table 1. The initial total hardness had a concentration ratio of 1:1 for $Ca^{2+}$ and $Mg^{2+}$. Batch experiments were performed according to the runs of CCD in 20 mL of the solution containing $Ca^{2+}$ and $Mg^{2+}$ ions in the binary ionic system. The content was agitated with a magnetic stirrer at 500 rpm. After the desired contact time, a sample was drawn off and then centrifuged (5 min, 3000 rpm). The supernatant was analyzed to measure $Ca^{2+}$ and $Mg^{2+}$. The percentage of total hardness removal was selected as the response. The removal efficiency (R) is expressed as Eq. (2).

$$\%R = \left( \frac{C_0 - C_e}{C_0} \right) * 100 \qquad (2)$$

where $C_0$ and $C_e$ are the initial and final concentration (mg L$^{-1}$) of ions, respectively.

*Competitive adsorption of $Ca^{2+}$ and $Mg^{2+}$*

The equilibrium exchange used to evaluate the competitive adsorption of $Ca^{2+}$ and $Mg^{2+}$ ions in the binary system. Amount of 0.08 g of nano LTA zeolite was added to the beakers containing 20 mL solutions in equal initial concentrations (150- 350 mgL$^{-1}$) of $Ca^{2+}$ and $Mg^{2+}$ ions at pH of 6, the temperature of 25 ºC and different contact times (3min-5h). Other experimental details were a similar procedure as described above in the batch adsorption studies section. The adsorption capacity

$Q_e$ (mol g$^{-1}$) is calculated according to the Eq. (3).

$$Q_e = \frac{(C_0 - C_e) V}{m} \qquad (3)$$

where, $C_0$ and $C_e$ are the initial and final concentration (mgL$^{-1}$) of ions, respectively; $V$ is the solution volume ($L$), and $m$ indicates the mass of the nano LTA zeolite (g).

In the binary system, the adsorption precedence of an adsorbent for one of the two metals is introduced by the separation factor $\alpha_2^1$, which is given by Eq. (4).

$$\alpha_2^1 = \frac{Q_{e,1} C_{e,2}}{Q_{e,2} C_{e,1}} \qquad (4)$$

where, $Q_{e,1}$ and $Q_{e,2}$ are the adsorption capacities of metals 1 and 2 at equilibrium, and $C_{e,1}$ and $C_{e,2}$ are the equilibrium concentrations of the metals.

## RESULTS AND DISCUSSION
*SEM of synthesized nano LTA zeolite*

To investigate the effect of temperature and aging time on the morphology of LTA, zeolite was synthesized in three temperatures (70, 90, 98 ºC) in different aging times (30, 48, 72, 96 h). Fig. 1 shows the SEM images of LTA synthesized at 70 ºC in various aging times. As can be seen, there are many agglomerate particles with nearly spherical morphology, while any specific cubic morphology [37] which shows the LTA was formed, cannot be identified. Furthermore, increasing aging time at this temperature did not solve the problem and the final morphology is still spherical. Therefore, this temperature (70 ºC) is not sufficient enough to synthesize the LTA zeolite. Fig. 2 illustrates the SEM micrograph of samples prepared at 90 ºC aged at 30, 48, 72 and 96 h. According to Fig. 2a, at 90 ºC and after 30 h, the cubic morphology was not formed yet. However, when the aging time increased, the morphology of samples was changed and the crystals of LTA appeared at 96 h (Fig. 2d) with the average size of (>100 nm). It is noteworthy that although in Fig. 2 (b-d) the LTA crystal is observed these crystals have been still embedded in amorphous aggregates (especially in Fig. 2 (b-c)) and need higher temperature or aging time to complete crystallization process.

Fig. 3(a-d) compares the SEM images of the samples treated at 98 ºC and aged similar to other samples. In Fig. 3(a-b), there are some crystals of LTA covered by amorphous agglomerate particles.

122

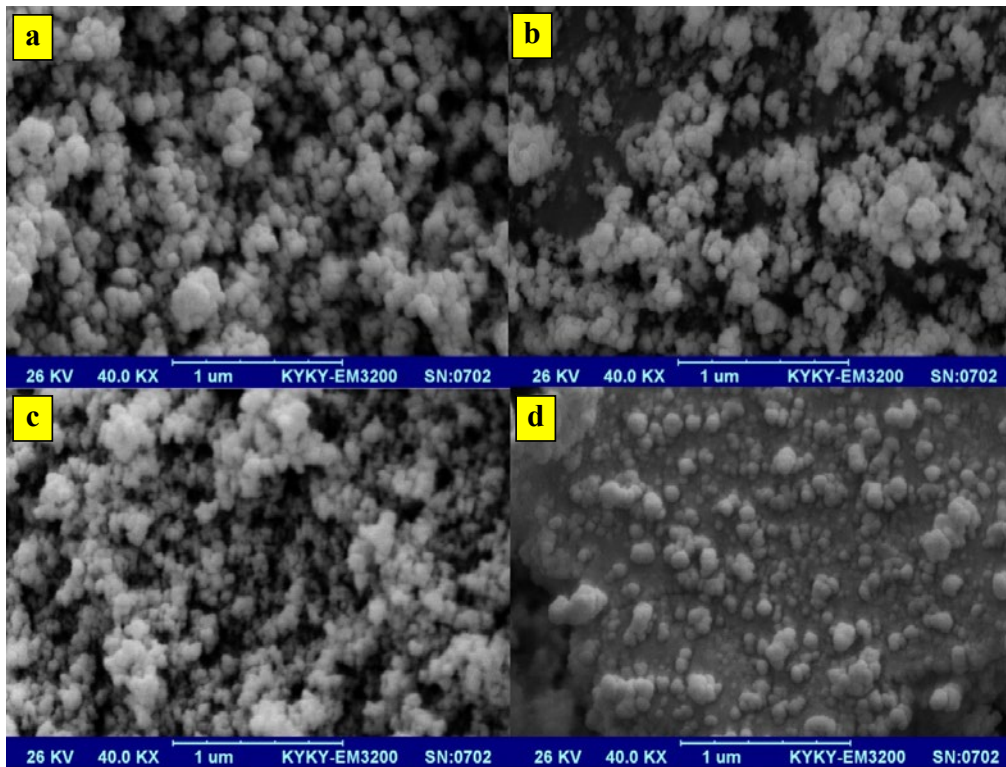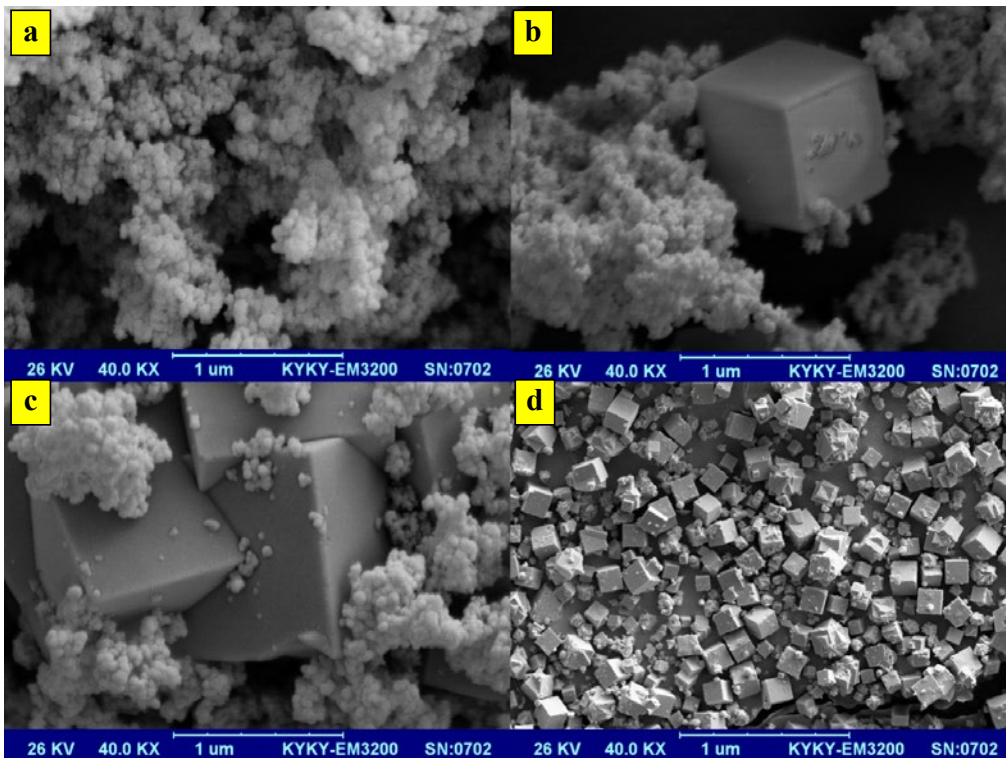*J. Water Environ. Nanotechnol., 4(2): 119-138 Spring 2019*

Fig. 1: SEM images of samples synthesized at 70 °C at different hydrothermal aging times. (a) 30 h, (b) 48h,(c) 72 h, (d) 96 h.



Fig. 2: SEM images of samples synthesized at 90 °C at different hydrothermal time. (a) 30 h,(b) 48 h, (c) 72 h, (d) 96 h.
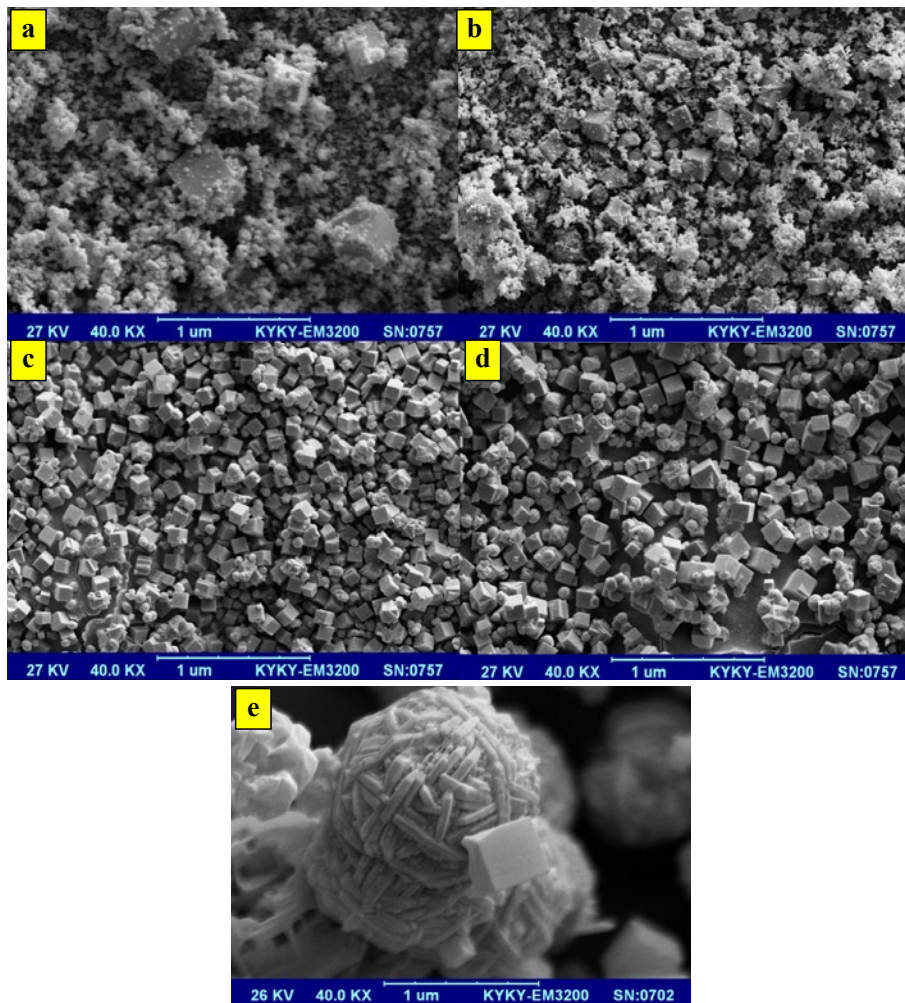
*J. Water Environ. Nanotechnol., 4(2): 119-138 Spring 2019*

123

Fig. 3: SEM images of samples synthesized at 98 ℃ at different hydrothermal time. (a) 30 h, (b) 48 h, (c) 72 h, (d) 96 h. (e) yarn ball like morphology.

It shows that more aging time needs to bring the material to the crystal phase [38]. However, increasing the aging time from 72 to 96 h helped crystallization, and the well-defined LTA cubic crystals were formed. Although in 96 h the cube shape is dominated, there are some spherulites owning "yarn-ball"-like morphology that corresponded to sodalite crystals. Therefore, it can be concluded that increasing aging time to 96 h can destruct LTA cubic morphology and converting it into sodalite crystals [37]. Fig. 3e clarifies the sodalite morphology which was selected from a zone in Fig. 3d.

To sum it up, in low temperatures e.g., 70 ℃, increasing aging time cannot be affected by the crystallization process to produce LTA with a characteristic cube shape. On the other hand, high temperature and more aging time can deform the cubic morphology and change to sodalite phase [39]. Therefore, there is an optimum condition (temperature and aging time) to prepare LTA zeolite
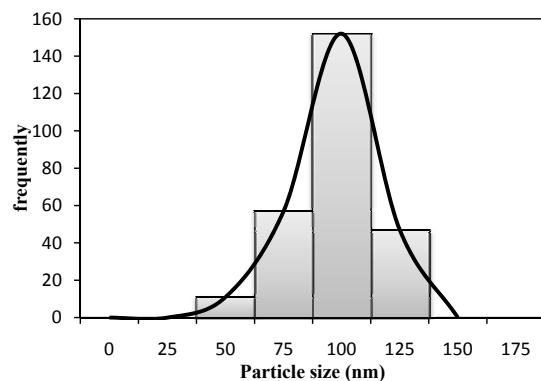


Fig. 4: Particles size distribution of nano LTA zeolite.

124

*J. Water Environ. Nanotechnol., 4(2): 119-138 Spring 2019*

with cubic crystals. The crystal size distribution of optimum sample (98 °C and 72 h) was measured and given in Fig. 4. The sample has crystals with sizes from 50 to 125 nm and an average size of 100 nm approximately. In light of these discussions, the sample was synthesized at 98 °C and aged at 72 h was selected for further characterization and application studies.

Fig. 5 demonstrated the EDS analysis of the LTA zeolite in optimum condition (98 °C and 72 h). According to Fig. 5, Si, Al, O, and Na were discovered as the significant elements in this sample. The semi-quantitative values of the ratios of Si/Al and Na/Si were calculated 0.86 and 0.89, respectively. What is more, the EDS analysis confirms the main existence of components of

nano LTA zeolite framework.

*XRD analysis*

Fig. 6 illustrates the XRD patterns of nano LTA zeolite prepared at 98 °C and aged at 72 h. As can be observed, the XRD pattern contains sharp and intense peaks. The peaks found in 2θ = 7.1°, 10°, 12.42°, 16.02°, 21.59°, 23.91°, 27.05°, 29.88° and 34.09° can correspond to LTA zeolite The average size of nano-crystallites was calculated according to the Debye- Scherrer equation (5) [40]:

$$D = \frac{K\lambda}{\beta\cos\theta} \qquad (5)$$

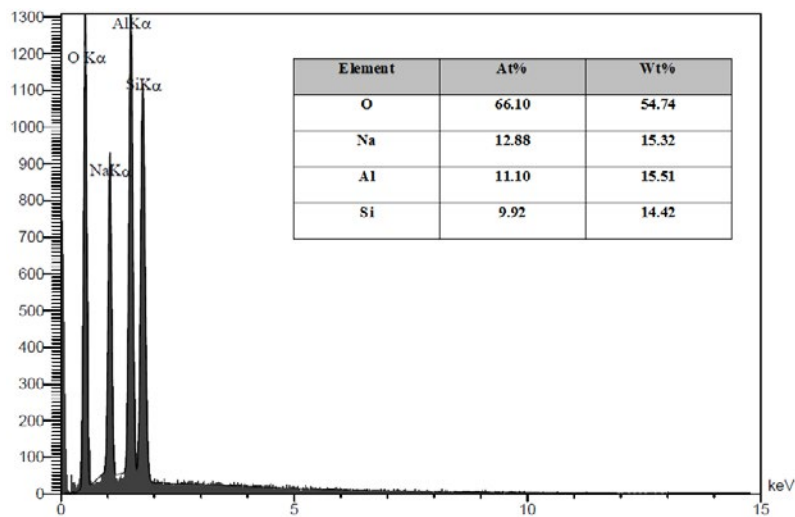where D is the average crystallite size in nm, K is crystallite shape factor (0.893), λ is the specific



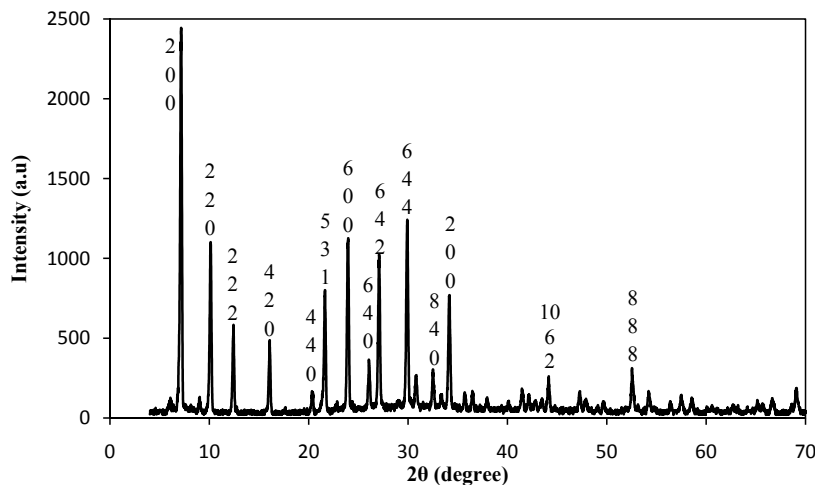Fig. 5: The EDS analysis of the sample synthesized at 98 °C, 72 h.



Fig. 6: XRD patterns of samples synthesized at 98 °C and 72 h.

*J. Water Environ. Nanotechnol., 4(2): 119-138 Spring 2019*

125

wavelength of X-ray beam ($\lambda_{CuKa} = 0.154nm$), θ is one-half of the diffraction angle (Braggs' angle, degree) and β is the full-width half maxima (FWHM) of maximum peak intensity. According to this definition for full width at half maximum of the most intense peak (2θ=7.19°) the average size of nano LTA zeolite was calculated to be about 43.26 nm.

The relative crystallinity of the synthesized sample was calculated using the total XRD peak intensities ratio of the reference LTA zeolite to the total peak intensities of synthesized zeolite by Eq. (6) [29]:

$$\text{Crystalinity (\%)} = \frac{\sum \text{Intensity of XRD peak of product}}{\sum \text{Intensity of XRD peak of standard}} \times 100 \quad (6)$$

The relative crystallinity of nano LTA zeolite was obtained, 83.1%, that confirmed the sample synthesized in single and high crystalline phases. The crystallinity was compared with other studies that had the same synthesis process (alkali fusion followed hydrothermal method) with a different source, temperature and crystallization time. The published values for crystallinity of zeolite 4A in literature was 61.8% (fly ash, 90 °C and 5 h) [29], 75.8% (fly ash, 90 C and 4 h) [25], 23% (oil shale ash, 100 °C and 72 h) [41] and 95% (fly ash, 80 °C and 24 h) [42]. The difference between the crystallinity values could be due to their different temperature and crystallization time. So that the optimal values of the temperature and crystallization time can lead to the synthesis of a more pure phase and cubic particles with uniform size distribution [39].

*FT-IR analysis*

To support the SEM results, the effects of temperature and aging times were also investigated by FTIR. The original IR bands which are the characteristic of LTA zeolite might be found in [43, 44]. They involving double ring vibrations (D4R), 500-650 cm⁻¹, pore opening vibrations, 1050-1150 cm⁻¹, and internal tetrahedral vibrations 920-1250 cm⁻¹. The fingerprint peak which confirmed the crystallization of LTA zeolite, is 500 to 600 cm⁻¹,
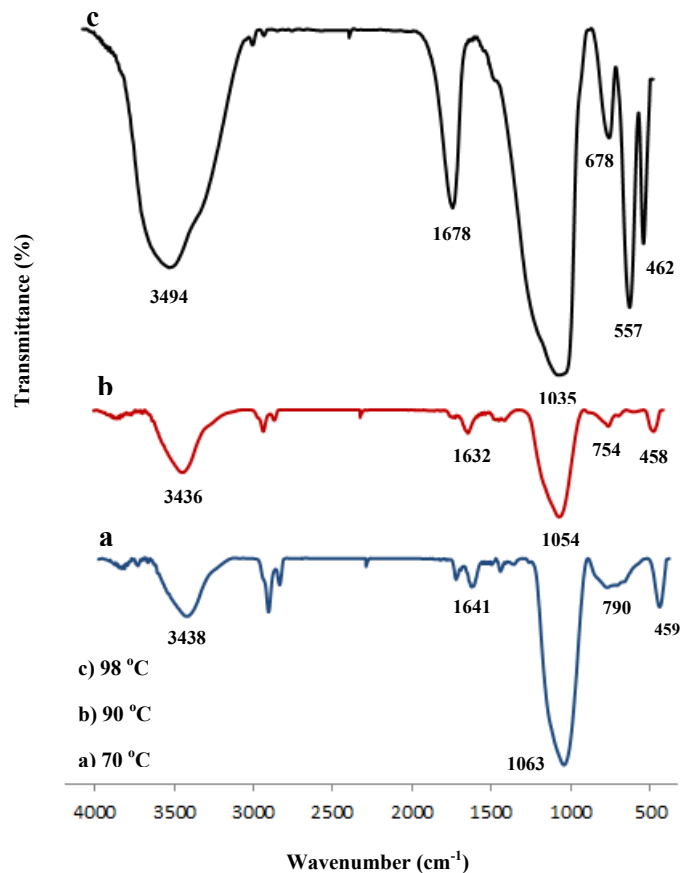


Fig. 7. FT-IR spectra of samples synthesized at 70, 90, 98 °C and 72 h.

that related to the presence of D4R [45].

Fig. 7 compares the FTIR spectra of the samples synthesized at 70, 90 and 98 °C aged in 72 h. As can be seen, the band situated at about 464 cm$^{-1}$ ascribed to the beginning of the crystallization of a zeolite with b-cage and the peak in the region from 500 to 600 cm$^{-1}$ has not been formed at temperature 70 °C (7a) or the band was very weak at temperature 90 °C (7b). Moreover, by increasing hydrothermal temperature to 98 °C (7C) the peak at about 547 cm$^{-1}$ appeared clearly and the intensity of the absorption band was strong; this figure indicated that a considerable amount of mass transformation of amorphous precursor gel into

crystalline LTA zeolite type and it was the majority phase in the synthesized samples since [D4R] only existed in LTA zeolite. Accordingly, it can be concluded that the temperatures of 70 or 90 °C are low to the synthesis of LTA zeolite with suitable cubic morphology. These results support those were obtained from SEM (Fig. 1 and Fig. 2).

More investigation was done with FTIR recodes of samples synthesized in 98 °C and aged in 30, 48, 72 and 96 h (Fig. 8 (a-d)). The weak band located in 500-650 cm$^{-1}$ (assigned to D4R) in Fig. 7a can represent the minority phase of LTA, supported with SEM micrograph of Fig. 3a. When the aging time increased (i.e. 48 and 72 h) the band at 500-
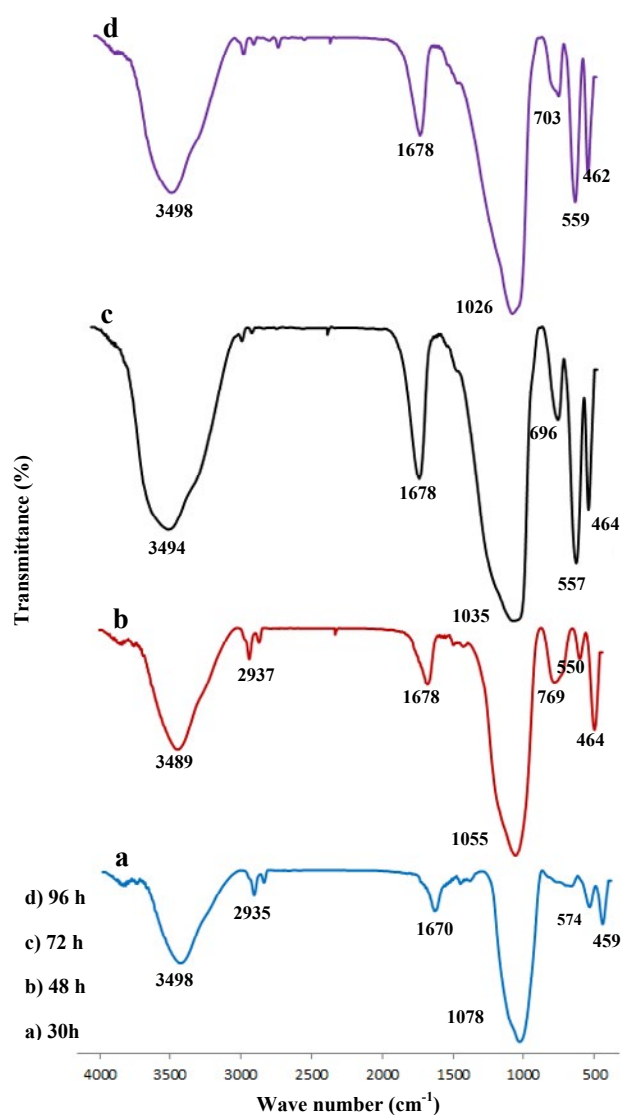


Fig. 8: FT-IR spectra of samples synthesized at 98 °C and crystallization times of 30, 48, 72 and 96 h.

*J. Water Environ. Nanotechnol., 4(2): 119-138 Spring 2019*

127

650 cm$^{-1}$ was intensified. However, when the sample aged in more time (96 h), this characteristic band (D4R) became weaker, which was suggesting that LTA zeolite has converted to SOD zeolite and transition from the cubic shape (LTA) to the spherical shape (sodalite). These results can be supported by the SEM image in Fig. 3 (e-d).

*TGA and DSC discussions*

Thermal analysis of the prepared nano LTA zeolite is useful in finding the right temperature range of its application because different zeolite systems are decomposed at different temperatures. Fig. 9 illustrates TGA-DSC diagram of nano LTA zeolite. The zeolite sample was tested by placing about 2.5 mg sample into a hermetic pan. The curve was done at a heating rate of 10 °C min$^{-1}$ over a temperature range of 30- 1200 °C. According to the TGA behavior, there was a slight decline in the mass sample by increasing temperature. The weight decrease (approximately 21.74 wt %) at temperature range 150- 400 °C is generally due to the removal of residual water, while losses at higher temperatures are related to the more tightly bounded molecules in the structure of zeolite [46]. The peaks observed in the DSC curve confirmed on the TGA curve. The DSC curve shows two weak endothermic peaks at about 150°C and above 400 °C, attributed to free and physically adsorbed water and the dehydration (destruction of hydroxyl bond) of water molecules

coordinated to sodium ions located in the α-cages and β-cages of the LTA zeolite framework , respectively [25, 47, 48].

*Nitrogen Adsorption/Desorption Analysis*

The BET model acts based on measuring the amount of N$_2$ adsorption/desorption using the surface of the material at 77 K of the constant liquid nitrogen. By using this model the specific surface area and pore size distribution of nano LTA zeolite were estimated.

The solid porous texture determines isotherm shape. According to the IUPAC classification of adsorption isotherms, Fig. 10a illustrates the microporous materials isotherms (type I), with H4 hysteresis loop. Steep isotherms at low pressures indicate that most micropores were filled at very low pressures. In addition, a broad capillary condensation taken placed between 0.03<P/P$_0$<0.96. The t-plot represented in Fig. 10b is the more reliable and most successful method to estimate total micropore volume. There are two slopes, a straight line with a slope correspondent to the surface area external to micropores and another is sharpness and passes from t = 0. The curvature of plots suggests that there is distribution in pore size [49, 50]. The useful data extracted from BET and t-plot curves of nano LTA zeolite are listed in Table 2. The measured specific surface area from the BET model (S$_{BET}$) and micropore volume (V$_p$) have a
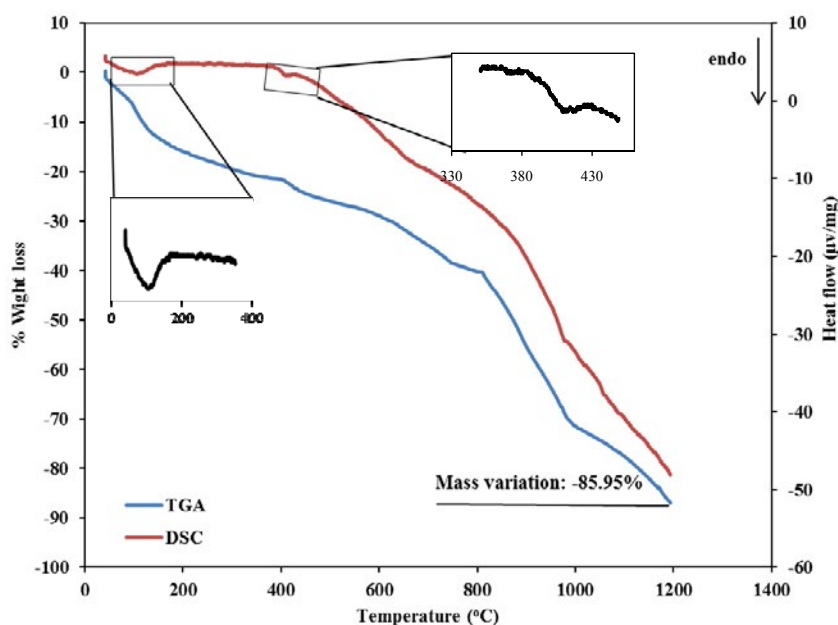


Fig. 9: TGA- DSC curves of the sample synthesized at 98 °C, 72 h.

128

*J. Water Environ. Nanotechnol., 4(2): 119-138 Spring 2019*

Table 3. Comparison between the specific surface areas of nano LTA zeolite with those reported in the literature.

| Sources | Synthesis method | Condition | $S_{BET}$ (m²/g) | Reference |
|---|---|---|---|---|
| Kaolin | hydrothermal | 18 h at 30 °C | 5.9 | [64] |
| Sodium metasilicate and sodium aluminate | microwave | 3–4 h at 99 °C. | 11.199 | [43] |
| Brazilian Coal Ash | hydrothermal | 1-4 h at 80°C | 42.58-32.38 | [65] |
| Rice Husk | hydrothermal | 3 day at 25 °C | 62.520 | [66] |
| coal fly ash | hydrothermal | 1.5-2.5 h 90-95 °C | 122 | [26] |
| fly ash | Alkali fusion+ hydrothermal | 4 h at 90 °C | 18.33 | [25] |
| fly ash | Alkali fusion+ hydrothermal | 24 h at 80 °C | 27 | [42] |
| Silica and alumina | Alkali fusion+ hydrothermal | 72h at 98 °C | 352.6 | Current work |
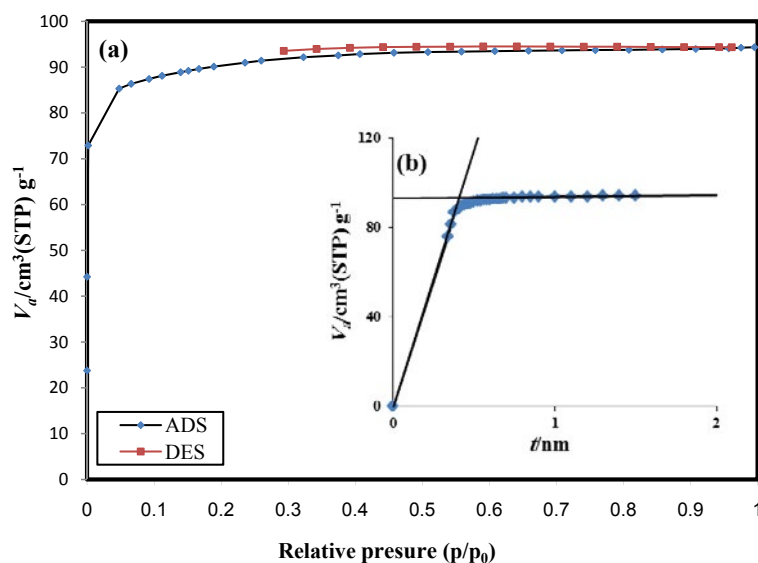


Fig. 10: N₂ adsorption-desorption test for nano LTA zeolite. (a) Isotherm (b) t-plot.

good match with that value ($a_1$) and $V_p$ obtained from t-plot.

Table 3 compared the specific surface area measured for nano LTA zeolite in this current work with reported values in the literature. The comparison was conducted based on time and crystallization temperature and method of synthesis of LTA zeolite. According to these values, the calculated $S_{BET}$ (352.52 m². g⁻¹) for nano LTA zeolite is by far than the others. In summary, the higher temperature and time of crystallization, pure starting materials and as well as the used method including alkali fusion along with hydrothermal, produced LTA zeolite with this high specific surface area in comparison with the reported ones.

*Competitive exchange of Ca²⁺ and Mg²⁺*

The separation factor ($\alpha_2^1$) was calculated to evaluate the performance of nano LTA zeolite for exchange that shows ion selectivity in the binary systems. Overall, $\alpha_2^1 > 1$ implies that adsorbent has preferred to metal 1 and $\alpha_2^1 < 1$ infers that adsorbent has preferred to metal 2. In this study number 1 is related to Ca²⁺ and 2 for Mg²⁺.[51]. Fig. 11 illustrates changes in the amount of the separation factor for Ca²⁺ and Mg²⁺ ions in different concentrations (75-425 mgL⁻¹) in the binary system.

As can be seen, there was a sharp rose in separation factor (more than 1) which means nano LTA zeolite has more affinity to Ca²⁺ than Mg²⁺. Firstly, this could be due to the ion exchange selectivity of zeolite frequently depends on the hydrated ionic radius. By increasing the ionic radii, the selectivity of zeolites decreases. On the other hand, the pores size of the nano LTA zeolite is different. The free diameter of the cavity of LTA is: (i) 2.3 A° for the four - rings (D-4), (ii) 6.6 A° for β-cage and (iii) 11.4 °A for the super cavity (α-cage)
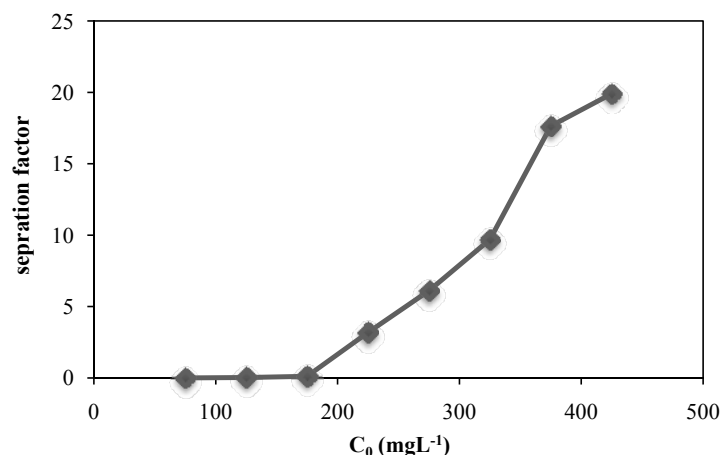
*J. Water Environ. Nanotechnol., 4(2): 119-138 Spring 2019*

129

Fig. 11. Separation factor ($\alpha_2^1$) as a function of total initial concentration with the initial concentration ratio of 1:1 Ca²⁺ and Mg²⁺.
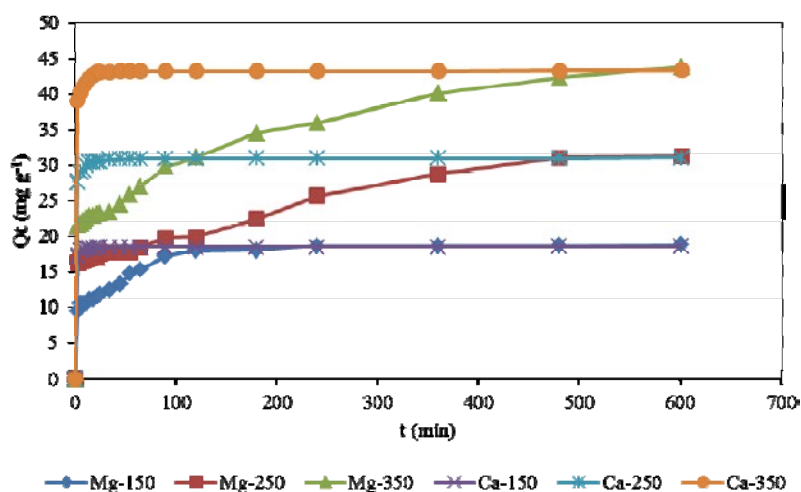


Fig. 12. The Ca²⁺ and Mg²⁺ competitive exchange data with different initial concentration.

[19]. Mg²⁺ ions may be located in $\alpha$-cages while Ca²⁺ ions more prefer the $\beta$-cage and D-4 sites where they can be hydrated with the maximum number of water molecules. Based on these results it can be concluded that the affinity sequence of nano LTA zeolite was determined as Ca²⁺> Mg²⁺ [52, 53]

The effect of competitive ions adsorption in the nano LTA zeolite was investigated using Ca²⁺ and Mg²⁺ ions in the binary system. Fig. 12 shows the influence of adsorption time on the adsorption capacity for different concentration. As can be seen, that adsorption capacity ions increased with the increasing initial concentration of Ca²⁺ and Mg²⁺ ions. According to Fig. 12, the maximum ion adsorption capacity at initial concentration 150, 250 and 350 mgL⁻¹ for Ca²⁺ is achieved roughly at 18, 30 and 41 min, respectively and for Mg²⁺ ion is

obtained about at 19, 31 and 600 min, respectively. It is evident that the adsorption rates of Ca²⁺ are faster than Mg²⁺ ions to exchange at 15 min and rapidly reached the equilibrium point.

Furthermore, the exchangeability of Ca²⁺ is higher than Mg²⁺ on nano LTA zeolite. As explained in the separation factor section, this is because Mg²⁺ exists in the form of hydrate in the solution, which makes it hard to exchange with Na⁺ in zeolite [30].

### The kinetics of removal of Ca²⁺ and Mg²⁺

The kinetics of ion exchange can provide information for the efficiency of sorption, the selection of the adsorbent and the exchange condition in a certain application. The controlling mechanism of sorption of Ca²⁺ and Mg²⁺ ions on the nano LTA zeolite in the binary system were

investigated by the pseudo-first-order and the pseudo-second-order kinetic models. In general, the pseudo-first-order model indicates the rapid period of the adsorption and the pseudo-second-order implies chemical adsorption nature. These models were given by Eq. (7) and (8) respectively:

$$\log(q_e - q_t) = \log q_e - (\frac{k_1}{2.303})t \qquad (7)$$

$$\frac{t}{q_t} = \frac{1}{k_2 q_e^2} + \frac{t}{q_e} \qquad (8)$$

Where $q_e$ [mg g$^{-1}$] and $q_t$ refer to the amounts of adsorption at the equilibrium and any time t [min] respectively. $k_1$[min$^{-1}$] and $k_2$ [g mg$^{-1}$ min$^{-1}$] are the adsorption rate constants in the pseudo-first-order adsorption and pseudo-second-order adsorption, respectively.

The kinetic parameters were obtained from fitting of the pseudo-first-order and pseudo-second-order models on ion-exchange data of Ca$^{2+}$ and Mg$^{2+}$ ions and were presented in Table 4.

The high correlation coefficient values (all 0.99) showed that the pseudo-second-order model fitted extremely well with experimental values rather than the pseudo-first-order model. On the other hand, the quantities of q$_{e, cal}$ of the pseudo-second-order model are only a little lower than q$_{e, exp}$. It can be concluded that the ion exchange process controlled via the chemical sorption being the rate-controlling step [54, 55].

### Results of CCD

Table 5. gives 29 random experiments to evaluate the optimum five variables at five levels for

Table 4. Kinetic parameters and correlation coefficients for fitting of pseudo first and second order model.

| Model | Parameters | Values of Parameters | | |
|---|---|---|---|---|
| | $C_0$ (mg L$^{-1}$) | 150 | 250 | 350 |
| | q$_{e,exp}$ (mg g$^{-1}$) | 37.49 | 62.13 | 87.33 |
| | q$_{e,cal}$ (mg g$^{-1}$) | 7.30 | 18.93 | 0.25 |
| Pseudo-first-order | $k_1$ (min$^{-1}$) | 0.05 | 0.005 | 0.03 |
| | $R^2$ | 0.64 | 0.74 | 0.97 |
| | q$_{e,cal}$ (mg g$^{-1}$) | 37.59 | 62.11 | 68.95 |
| Pseudo-second-order | $k_1$ (min$^{-1}$) | 0.005 | 0.001 | 0.001 |
| | $R^2$ | 0.99 | 0.99 | 0.99 |

Table 5. Matrix of experimental design, experimental response and model predicted values.

| Run | Factors | | | | | Responses | |
|---|---|---|---|---|---|---|---|
| | $x_1$ | $x_2$ | $x_3$ | $x_4$ | $x_5$ | Predicated R % | Observed R % |
| 1 | 4 | 0.11 | 300 | 17 | 90 | 76.44 | 75.66 |
| 2 | 4 | 0.05 | 200 | 17 | 90 | 44.24 | 43.05 |
| 3 | 6 | 0.08 | 250 | 35 | 65 | 80.62 | 82.9 |
| 4 | 6 | 0.08 | 350 | 23 | 65 | 89.56 | 86.56 |
| 5 | 6 | 0.08 | 250 | 23 | 15 | 54.78 | 47.11 |
| 6 | 6 | 0.08 | 250 | 23 | 65 | 63.5 | 65.58 |
| 7 | 6 | 0.08 | 250 | 23 | 115 | 72.22 | 74.23 |
| 8 | 6 | 0.08 | 250 | 23 | 65 | 63.5 | 63.87 |
| 9 | 8 | 0.11 | 200 | 17 | 90 | 85.36 | 82.94 |
| 10 | 8 | 0.05 | 200 | 29 | 90 | 75.72 | 72.11 |
| 11 | 4 | 0.05 | 200 | 29 | 40 | 48.64 | 49.78 |
| 12 | 10 | 0.08 | 250 | 23 | 65 | 67.74 | 68.46 |
| 13 | 4 | 0.11 | 200 | 17 | 40 | 58.28 | 57.41 |
| 14 | 8 | 0.05 | 300 | 17 | 90 | 55.8 | 60.2 |
| 15 | 6 | 0.14 | 250 | 23 | 65 | 87.98 | 95.75 |
| 16 | 4 | 0.05 | 300 | 17 | 40 | 56.69 | 56 |
| 17 | 6 | 0.08 | 250 | 23 | 65 | 63.5 | 61.62 |
| 18 | 8 | 0.05 | 200 | 17 | 40 | 46.24 | 50.1 |
| 19 | 6 | 0.08 | 150 | 23 | 65 | 86.72 | 89.96 |
| 20 | 4 | 0.11 | 200 | 29 | 90 | 95.56 | 94.52 |
| 21 | 6 | 0.02 | 250 | 23 | 65 | 39.02 | 39.63 |
| 22 | 4 | 0.05 | 300 | 29 | 90 | 71.36 | 71.06 |
| 23 | 2 | 0.08 | 250 | 23 | 65 | 59.26 | 57.11 |
| 24 | 6 | 0.08 | 250 | 11 | 65 | 46.38 | 43.06 |
| 25 | 8 | 0.11 | 300 | 17 | 40 | 65.48 | 66.46 |
| 26 | 4 | 0.11 | 300 | 29 | 40 | 88.84 | 93.2 |
| 27 | 8 | 0.11 | 200 | 29 | 40 | 97.56 | 94.89 |
| 28 | 8 | 0.05 | 300 | 29 | 40 | 60.4 | 63.73 |
| 29 | 8 | 0.11 | 300 | 29 | 90 | 87.68 | 80.38 |

*J. Water Environ. Nanotechnol., 4(2): 119-138 Spring 2019*

131

predicting the performance removal hardness. To get the main effect of factors and their interactions, analysis of variance (ANOVA) was performed. The confidence level of 95% was chosen. Therefore, the p-value less than 0.05 in the ANOVA table revealed that the factor is significant in the adsorption process. All significant terms in the quadratic model were identified using F-test. The F-value of the model should be greater than the tabulated one for a certain degree of freedom and p-value [35]. Table 6. presents the ANOVA results of this study. As can be observed, the model F-value was achieved as 36.90, which can be considered a significant value. Furthermore, P-value corresponding to the F-value of the model is very low (0.0001<0.05) and is also significant. However, the corresponding p-value for "Lack of Fit" is insignificant which confirms that the model fitted well on the data.

Moreover, the values of 0.96, 0.86 and 0.93 corresponding to the determination coefficient $R^2$, predicated $R^2$ and the adjusted $R^2$, respectively,

displays the suitability of the model for predicting the true behavior of adsorption process. The acceptable standard deviation, low coefficient of variation and good value of the mean, reveal the goodness and applicability of the model.

The p-value of all terms involved in the model is given in Table 6. In this case, the pH ($x_1$), adsorbent dosage ($x_2$), temperature ($x_4$) and contact time ($x_5$) are key parameters. Interaction terms such as $x_1x_3$, $x_2x_3$, and one quadratic term $x_3^2$ are also significant. In contrast, initial total hardness ($x_3$) and other interaction terms ($x_2x_4$, $x_3x_4$, $x_3x_5$) have less importance and are insignificant to the response.

The residual analysis used to prove the precision and assumptions for the ANOVA. Fig. 13a illustrates the normal probability plot versus residual values. The data nearly straight line and the least deviation showed a good relationship between selected factors and response. Also, described suitability of the model for experimental

Table 6. ANOVA for the fit of the experimental data to the response surface model.

| Source of variations | Degrees of freedom | Sum of squares | Mean square | F-value | P-value |
|---|---|---|---|---|---|
| Model | 7798.7 | 11 | 703.52 | 36.9 | < 0.0001 |
| $x_1$ | 107.65 | 1 | 107.65 | 5.65 | 0.0295 |
| $x_2$ | 9593.42 | 1 | 3593.42 | 188.46 | < 0.0001 |
| $x_3$ | 12.17 | 1 | 12.17 | 0.64 | 0.4354 |
| $x_4$ | 1760.10 | 1 | 1760.10 | 92.31 | < 0.0001 |
| $x_5$ | 455.79 | 1 | 455.79 | 23.90 | 0.0001 |
| $x_1x_3$ | 424.67 | 1 | 424.67 | 22.27 | 0.0002 |
| $x_2x_3$ | 144.06 | 1 | 144.06 | 7.56 | 0.0137 |
| $x_2x_4$ | 60.8 | 1 | 60.8 | 3.19 | 0.0920 |
| $x_3x_4$ | 55.32 | 1 | 55.32 | 2.90 | 0.1067 |
| $x_3x_5$ | 58.26 | 1 | 58.26 | 3.06 | 0.0985 |
| $x_3^2$ | 1066.46 | 1 | 1066.46 | 55.93 | < 0.0001 |
| Residual Error | 324.15 | 17 | 19.07 | - | - |
| Lack-of-fit | 316.26 | 15 | 21.08 | 5.34 | 0.1687 |
| Pure error | 7.89 | 2 | 3.94 | - | - |
| Total | 8062.06 | 28 | - | - | - |
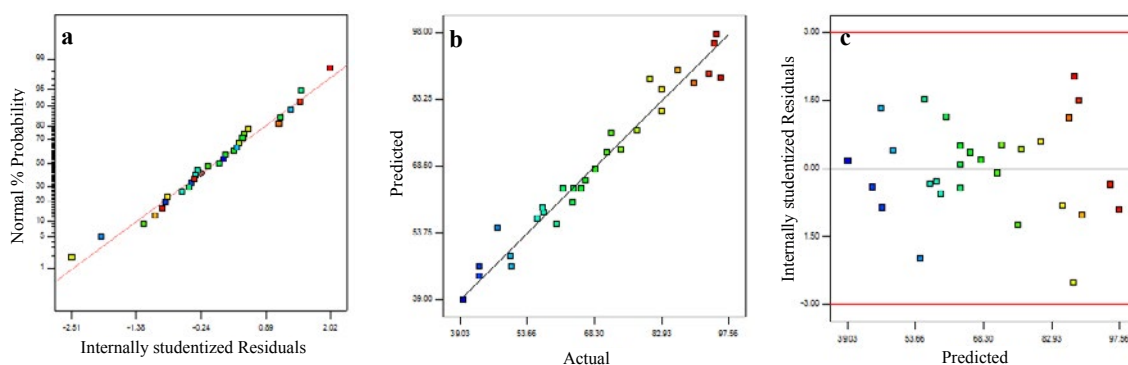


Fig. 13. Residual analysis (a) Normal Plot of Residuals, (b) Predicted Plot vs. Actual, (c) Residuals Plot vs. Predicted.

132

*J. Water Environ. Nanotechnol., 4(2): 119-138 Spring 2019*

data. The predicted versus the experimental values were plotted in Fig. 13b. The correlation coefficient that presented in Table 6 for this figure indicates the good fitting capability of the obtained model. Fig. 13c demonstrates the residual values versus the predicted values. Random scatter of points and their distribution between -3 and +3 showed reasonably distribution and good fitting for the model [56, 57].

Based on these results, the quadratic model that presents the functionality of total removal hardness to the selected factors derived as:

$$y = 63.5 + 2.12x_1 + 12.24x_2 + 0.71x_3 + 8.56x_4 + 4.3$$
$$-5.15x_1x_3 - 3x_2x_3 + 1.95x_2x_4 - 1.86x_3x_4 - 1.91x_3x_5 + 6.16x_3^2$$

It should be noted that the model was given a base on the coded values of factors. The magnitude of coefficients reveals that a variable impact on the response.

In this case, adsorbent dosage ($x_2$) and temperature ($x_4$) have the highest positive effect in comparison with pH ($x_1$) and contact time ($x_5$). According to the results of the analysis of ANOVA, the highest interactions effect were found for $x_1x_3$

and $x_2x_3$. While the other three terms variable interactions have not a consequential effect on the total hardness removal.

To more investigations, the interactive effect of two factors used in the 3D response surfaces and the corresponding contour plots (Fig. 14).

As can be seen from Fig. 14 (a,b), the response enhanced by increasing $x_1$ (pH) and decreasing $x_3$ (initial total hardness). The highest response can be obtained when the $x_1$ and $x_3$ variables were at their maximum and minimum values within the studied range, respectively.

Typically by increasing pH, the adsorption of $Ca^{2+}$ and $Mg^{2+}$ ions increases. As shown in Fig. 14 (a,b), total hardness removal from solution achieves to a maximum amount when shifting pH ($x_1$) to alkali region (from 2 to about 10). However, the removal of total hardness decreases at the acidic media. It may be attributed by this fact that an abundance of proton concentration a considerable repulsive force and competition between $Ca^{2+}$ and $Mg^{2+}$ ions and $H^+$. Nevertheless, the increase in solution pH may cause the shift from ion exchange to chelation binding mechanism for calcium and magnesium ions. [58, 59].
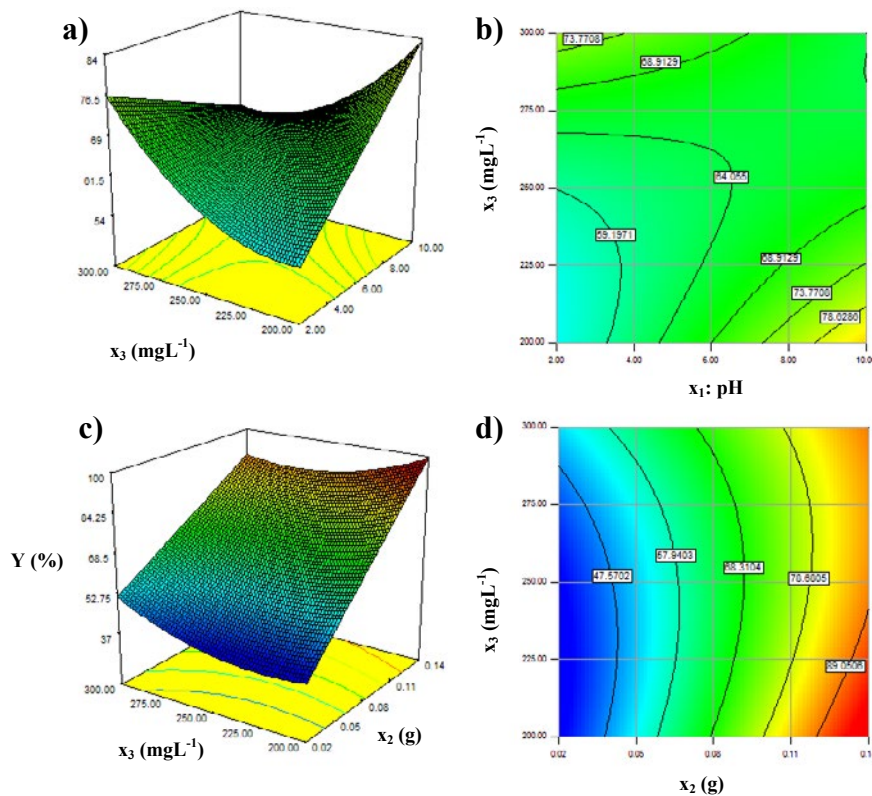


Fig. 14. Response surfaces and contour plots of central composite design: (a, b) $x_1$-$x_3$, (c, d) $x_2$-$x_3$.

*J. Water Environ. Nanotechnol., 4(2): 119-138 Spring 2019*

133

What is more, the total percent removal of hardness decreases with rising concentration $(x_3)$. This fact may be related to the high available number of $Ca^{2+}$ and $Mg^{2+}$ ions per unit mass of adsorbent and finally saturation of available surface area by calcium and magnesium ions as well [60].

According to Fig. 14 (c-d), a high adsorbent dosage $(x_2)$ and a low concentration of $Ca^{2+}$ and $Mg^{2+}$ $(x_3)$ give a high value of the response.

It is evident (Fig. 13c) that raising of adsorbent dosage causes an increase in surface area and accessibility of more active sites and finally result in the increase of the $Ca^{2+}$ and $Mg^{2+}$ removal percentage [61].

The Pareto chart (Fig. 15), demonstrates the significance of each parameter on the response (the removal of total hardness). This chart depicted in sequential order in the form of percentage influence of main parameters, squared factors, and the interaction factors. It is clear that the most important factor is the main effect of adsorbent dosage $(x_2)$ on the other hand, other parameters
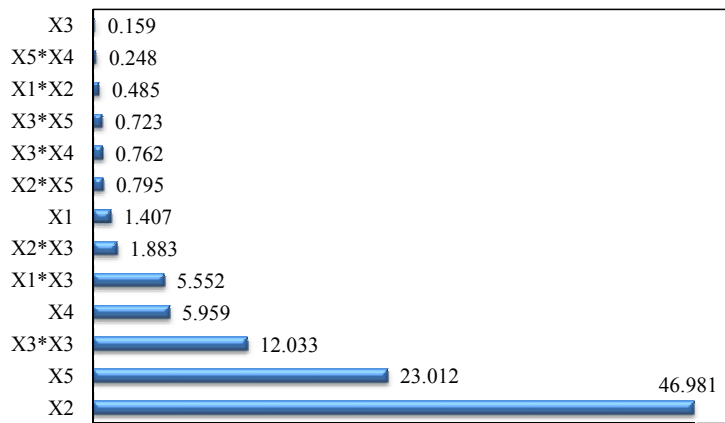


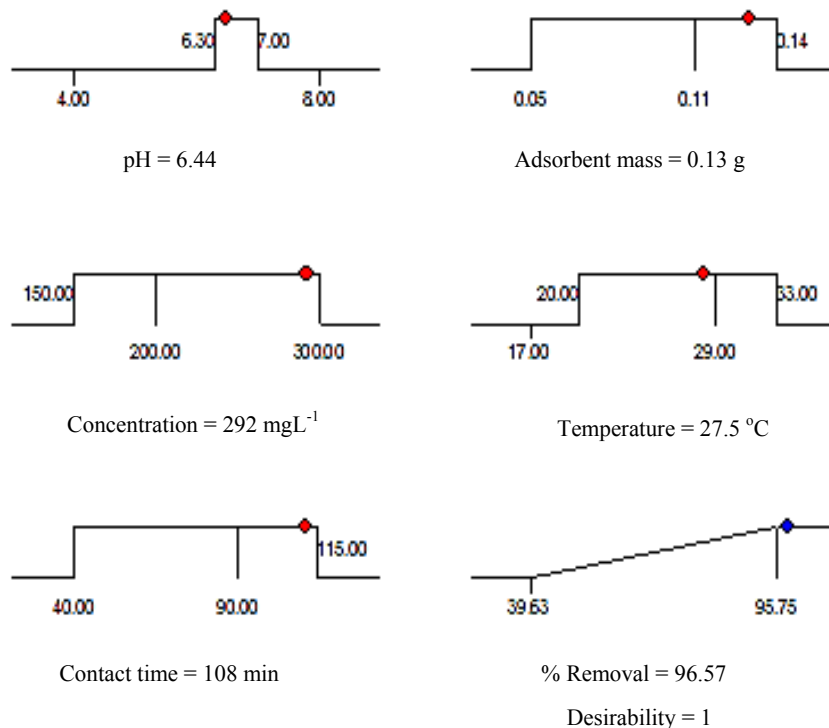Fig. 15. Standardized Pareto chart of total hardness removal.



pH = 6.44

Adsorbent mass = 0.13 g

Concentration = 292 mgL$^{-1}$

Temperature = 27.5 $^{\circ}$C

Contact time = 108 min

% Removal = 96.57

Desirability = 1

Fig. 16. Desirability ramp for optimization of five parameters.

134

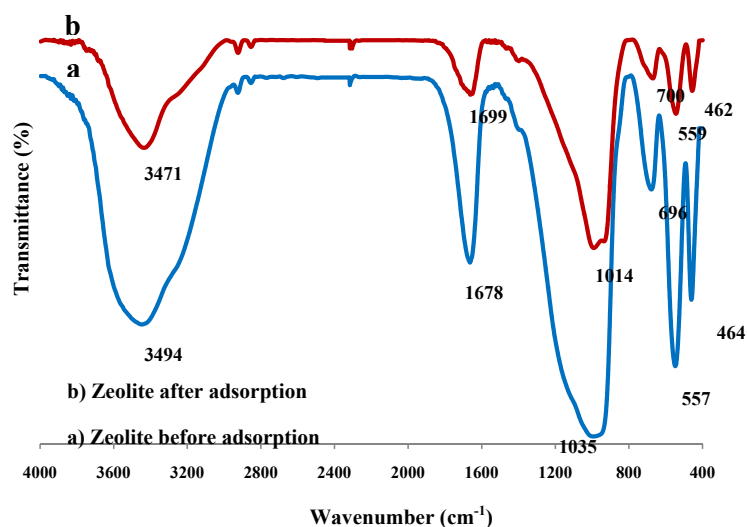*J. Water Environ. Nanotechnol., 4(2): 119-138 Spring 2019*

Fig. 17. FTIR of nano LTA zeolite before and after ion exchange process

include contact time ($x_5$), temperature ($x_4$) and interaction two factors (i.e., $x_3x_3$ and $x_1x_3$) have less significant than ($x_2$) [62].

*Optimization of the adsorption process*

The optimization of the process has been considered according to the environmental situation. Chosen environmental situations were corresponding to consist of pH of 6.42, the adsorbent dosage of 0.13 gL$^{-1}$, the initial concentration of 292 mgL$^{-1}$, the temperature of 27.5°C and contact time of 108 min (Fig. 16). To confirm efficient optimum reaction conditions obtained the desirability function. Optimum conditions were experimentally evaluated, and it was obtained observed that the total hardness removal percentage in the experiment (94.5%) was close to one observed from the model (96.6%). The desirability of the optimum solutions (Desirability = 1) illustrates the exactness between recommended solutions and experimental results. Additionally, this result verified that CCD design could be effectively used to optimize the adsorption parameters for the removal of total hardness [63].

## CHARACTERIZATION OF NANO LTA AFTER THE ION EXCHANGE PROCESS

In order to more investigate the ion exchange process in the nano LTA zeolite, FTIR was recorded before and after ion exchange. It is obvious from Fig. 17 that the characteristic bands in FTIR spectra have some shift to the lower wave numbers. However, the intensity of this band decreased after the ion exchange process. Therefore, it can be

concluded that all of the active sites are involved in the ion exchange process.

## CONCLUSION

In the current study, the nano LTA zeolite with good crystallinity and cubic morphology was synthesized at 98 °C for 72 h aging time, by alkaline fusion method without adding an organic template. Simultaneous removal Ca$^{2+}$ and Mg$^{2+}$ from water were studied. According to the competitive exchange data, nano LTA zeolite possesses a large amount of Ca$^{2+}$ ions, and also Ca$^{2+}$ competes with Mg$^{2+}$ in the adsorption process.

Optimization of the variables for maximum removal efficiency by nano LTA zeolite was performed using the quadratic model. The result showed that the operating pH, adsorbent amount, temperature and contact time had a significant impact on the removal efficiency (%). However, initial total hardness had not a significant influence on the response. The maximum removal of hardness (> 95%) was obtained at pH 6, the initial total hardness of 250 mg L$^{-1}$, absorbent amount of 0.14 g, a solution temperature of 23 °C and contact time of 65 min.

## CONFLICT OF INTEREST

The authors declare that there are no conflicts of interest regarding the publication of this manuscript.

*J. Water Environ. Nanotechnol., 4(2): 119-138 Spring 2019*

135

## REFERENCES

1. S.D. Faust, O.M. Aly, Chemistry of water treatment. (2018) CRC Press.

2. Kadir NNA, Shahadat M, Ismail S. Formulation study for softening of hard water using surfactant modified bentonite adsorbent coating. Applied Clay Science. 2017;137:168-75.

3. Brastad KS, He Z. Water softening using microbial desalination cell technology. Desalination. 2013;309:32-7.

4. P. Sengupta, Potential health impacts of hard water, *International journal of preventive medicine*. 4 (2013) 866.

5. M.F. Hiji, J.W. Ntalikwa, Investigations of Dodoma municipal hard water:(Part 1): Review of hard water treatment processes and identification of contaminants, International *Journal of Environmental Monitoring and Protection*. 1 (2014) 56.

6. Lazar L, Bulgariu L, Bandrabur B, Tataru-Farmus R-E, Drobota M, Gutt G. FTIR Analysis of Ion Exchange Resins with Application in Permanent Hard Water Softening. Environmental Engineering and Management Journal. 2014;13(9):2145-52.

7. Kazadi Mbamba C, Tait S, Flores-Alsina X, Batstone DJ. A systematic study of multiple minerals precipitation modelling in wastewater treatment. Water Research. 2015;85:359-70.

8. Mountadar S, Hayani A, Rich A, Siniti M, Tahiri S. Equilibrium, kinetic, and thermodynamic studies of the Ca2+ and Mg2+ ions removal from water by Duolite C206A. Solvent Extraction and Ion Exchange. 2018;36(3):315-29.

9. Zhang H-Z, Xu Z-L, Ding H, Tang Y-J. Positively charged capillary nanofiltration membrane with high rejection for Mg2 + and Ca2 + and good separation for Mg2 + and Li +. Desalination. 2017;420:158-66.

10. Zhang Z, Chen A. Simultaneous removal of nitrate and hardness ions from groundwater using electrodeionization. Separation and Purification Technology. 2016;164:107-13.

11. Chang Y-R, Lee Y-J, Lee D-J. Membrane fouling during water or wastewater treatments: Current research updated. Journal of the Taiwan Institute of Chemical Engineers. 2019;94:88-96.

12. Zhang W, Miao M, Pan J, Sotto A, Shen J, Gao C, et al. Separation of divalent ions from seawater concentrate to enhance the purity of coarse salt by electrodialysis with monovalent-selective membranes. Desalination. 2017;411:28-37.

13. Rashed MN, Palanisamy PN. Introductory Chapter: Adsorption and Ion Exchange Properties of Zeolites for Treatment of Polluted Water. Zeolites and Their Applications: InTech; 2018.

14. Ghasemi Z, Sourinejad I, Kazemian H, Rohani S. Application of zeolites in aquaculture industry: a review. Reviews in Aquaculture. 2016;10(1):75-95.

15. Nakhli SAA, Delkash M, Bakhshayesh BE, Kazemian H. Application of Zeolites for Sustainable Agriculture: a Review on Water and Nutrient Retention. Water, Air, & Soil Pollution. 2017;228(12).

[16] J. Behin, E. Ghadamnan, H. Kazemian, Recent advances in natural zeolites sciences and technologies in Iran, Clay Minerals - (2019) 1-54.

17. Wibowo E, Rokhmat M, Sutisna, Khairurrijal, Abdullah M. Reduction of seawater salinity by natural zeolite (Clinoptilolite): Adsorption isotherms, thermodynamics and kinetics. Desalination. 2017;409:146-56.

18. A. Fahmy, H. Youssef, A. Elzaref, Adsorption of Cadmium Ions onto Zeolite-A prepared from Egyptian Kaolin using Microwave, Int J Sci Res. 5 (2016) 1549-1555.

19. Xu R, Pang W, Yu J, Huo Q, Chen J. Chemistry of Zeolites and Related Porous Materials: John Wiley & Sons, Ltd; 2007 2007/07/18.

20. Czarna D, Baran P, Kunecki P, Panek R, Żmuda R, Wdowin M. Synthetic zeolites as potential sorbents of mercury from wastewater occurring during wet FGD processes of flue gas. Journal of Cleaner Production. 2018;172:2636-45.

21. Sharma P, Yeo J-g, Yu J-h, Han MH, Cho CH. Effect of ethanol as an additive on the morphology and crystallinity of LTA zeolite. Journal of the Taiwan Institute of Chemical Engineers. 2014;45(2):689-704.

22. Ezzeddine Z, Batonneau-Gener I, Pouilloux Y. Cation Exchange Mechanism of Divalent Metals ions onto Synthetic NaX and LTA Zeolites: Efficiency and Selectivity. European Chemical Bulletin. 2018;7(3):93.

23. Wen J, Dong H, Zeng G. Application of zeolite in removing salinity/sodicity from wastewater: A review of mechanisms, challenges and opportunities. Journal of Cleaner Production. 2018;197:1435-46.

24. Kazemian H, Naghdali Z, Ghaffari Kashani T, Farhadi F. Conversion of high silicon fly ash to Na-P1 zeolite: Alkaline fusion followed by hydrothermal crystallization. Advanced Powder Technology. 2010;21(3):279-83.

25. Liu Y, Yan C, Qiu X, Li D, Wang H, Alshameri A. Preparation of faujasite block from fly ash-based geopolymer via in-situ hydrothermal method. Journal of the Taiwan Institute of Chemical Engineers. 2016;59:433-9.

26. Iqbal A, Sattar H, Haider R, Munir S. Synthesis and characterization of pure phase zeolite 4A from coal fly ash. Journal of Cleaner Production. 2019;219:258-67.

[27] C. A. Ríos, C.D. Williams, O.M. Castellanos, Crystallization of low silica Na-A and Na-X zeolites from transformation of kaolin and obsidian by alkaline fusion, *Ingeniería y competitividad*. 14 (2012) 125-137.

28. Ayele L, Pérez-Pariente J, Chebude Y, Díaz I. Conventional versus alkali fusion synthesis of zeolite A from low grade kaolin. Applied Clay Science. 2016;132-133:485-90.

29. Lee M-G, Park J-W, Kam S-K, Lee C-H. Synthesis of Na-A zeolite from Jeju Island scoria using fusion/hydrothermal method. Chemosphere. 2018;207:203-8.

30. Xue Z, Li Z, Ma J, Bai X, Kang Y, Hao W, et al. Effective removal of Mg2+ and Ca2+ ions by mesoporous LTA zeolite. Desalination. 2014;341:10-8.

31. El-Rahman KMA, El-Kamash AM, El-Sourougy MR, Abdel-Moniem NM. Thermodynamic modeling for the removal of Cs+, Sr2+, Ca2+and Mg2+ions from aqueous waste solutions using zeolite A. Journal of Radioanalytical and Nuclear Chemistry. 2006;268(2):221-30.

32. Kolaei M, Dashtian K, Rafiee Z, Ghaedi M. Ultrasonic-assisted magnetic solid phase extraction of morphine in urine samples by new imprinted polymer-supported on MWCNT-Fe 3 O 4 -NPs: Central composite design optimization. Ultrasonics Sonochemistry. 2016;33:240-8.

33. Gandolfi F, Malleret L, Sergent M, Doumenq P. Parameters

136

*J. Water Environ. Nanotechnol., 4(2): 119-138 Spring 2019*

optimization using experimental design for headspace solid phase micro-extraction analysis of short-chain chlorinated paraffins in waters under the European water framework directive. Journal of Chromatography A. 2015;1406:59-67.

34. Asadzadeh F, Maleki-Kaklar M, Soiltanalinejad N, Shabani F. Central Composite Design Optimization of Zinc Removal from Contaminated Soil, Using Citric Acid as Biodegradable Chelant. Scientific Reports. 2018;8(1).

[35] D.C. Montgomery, Design and analysis of experiments, John Wiley & Sons. (2017).

36. Hesas RH, Baei MS, Rostami H, Gardy J, Hassanpour A. An investigation on the capability of magnetically separable Fe3O4/mordenite zeolite for refinery oily wastewater purification. Journal of Environmental Management. 2019;241:525-34.

37. Liu X-d, Wang Y-p, Cui X-m, He Y, Mao J. Influence of synthesis parameters on NaA zeolite crystals. Powder Technology. 2013;243:184-93.

38. Moheb Shahrestani M, Moheb A, Ghiaci M. High performance dehydration of ethyl acetate/water mixture by pervaporation using NaA zeolite membrane synthesized by vacuum seeding method. Vacuum. 2013;92:70-6.

39. Li Y, Peng T, Man W, Ju L, Zheng F, Zhang M, et al. Hydrothermal synthesis of mixtures of NaA zeolite and sodalite from Ti-bearing electric arc furnace slag. RSC Advances. 2016;6(10):8358-66.

[40] H. P. Klug, L.E. Alexander, X-ray diffraction procedures: for polycrystalline and amorphous materials. X-Ray Diffraction Procedures: For Polycrystalline and Amorphous Materials, 2nd Edition, by Harold P. Klug, Leroy E. Alexander, pp. 992., Wiley-VCH, May 1974., (1974) 992.

41. Fernandes Machado NRC, Malachini Miotto DM. Synthesis of Na–A and –X zeolites from oil shale ash. Fuel. 2005;84(18):2289-94.

42. Feng W, Wan Z, Daniels J, Li Z, Xiao G, Yu J, et al. Synthesis of high quality zeolites from coal fly ash: Mobility of hazardous elements and environmental applications. Journal of Cleaner Production. 2018;202:390-400.

43. Ghasemi M, Javadian H, Ghasemi N, Agarwal S, Gupta VK. Microporous nanocrystalline NaA zeolite prepared by microwave assisted hydrothermal method and determination of kinetic, isotherm and thermodynamic parameters of the batch sorption of Ni (II). Journal of Molecular Liquids. 2016;215:161-9.

44. Mukherjee S, Barman S, Halder G. Fluoride uptake by zeolite NaA synthesized from rice husk: Isotherm, kinetics, thermodynamics and cost estimation. Groundwater for Sustainable Development. 2018;7:39-47.

45. Noroozi R, Al-Musawi TJ, Kazemian H, Kalhori EM, Zarrabi M. Removal of cyanide using surface-modified Linde Type-A zeolite nanoparticles as an efficient and eco-friendly material. Journal of Water Process Engineering. 2018;21:44-51.

46. Tounsi H, Mseddi S, Djemel S. Preparation and characterization of Na-LTA zeolite from Tunisian sand and aluminum scrap. Physics Procedia. 2009;2(3):1065-74.

[47] J. Muller, G. Hakvoort, J. Jansen, DSC and TG Study

of Water Adsorption and Desorption on Zeolite NaA Powder and attached as layer on metal, *Journal of Thermal Analysis and Calorimetry*. 53 (1998) 449-466.

48. Musyoka NM, Petrik LF, Hums E, Kuhnt A, Schwieger W. Thermal stability studies of zeolites A and X synthesized from South African coal fly ash. Research on Chemical Intermediates. 2013;41(2):575-82.

49. Bandarchian F, Anbia M. Conventional hydrothermal synthesis of nanoporous molecular sieve 13X for selective adsorption of trace amount of hydrogen sulfide from mixture with propane. Journal of Natural Gas Science and Engineering. 2015;26:1380-7.

50. Leofanti G, Padovan M, Tozzola G, Venturelli B. Surface area and pore texture of catalysts. Catalysis Today. 1998;41(1-3):207-19.

51. Liu W, Wang T, Borthwick AGL, Wang Y, Yin X, Li X, et al. Adsorption of Pb2+, Cd2+, Cu2+ and Cr3+ onto titanate nanotubes: Competition and effect of inorganic ions. Science of The Total Environment. 2013;456-457:171-80.

52. Barri SAI, Rees LVC. Binary and ternary cation exchange in zeolites. Journal of Chromatography A. 1980;201:21-34.

53. Xue Z, Ma J, Hao W, Bai X, Kang Y, Liu J, et al. Synthesis and characterization of ordered mesoporous zeolite LTA with high ion exchange ability. J Mater Chem. 2012;22(6):2532-8.

54. Qin C, Wang R, Ma W. Adsorption kinetic studies of calcium ions onto Ca-Selective zeolite. Desalination. 2010;259(1-3):156-60.

55. Zayed AM, Selim AQ, Mohamed EA, Abdel Wahed MSM, Seliem MK, Sillanpää M. Adsorption characteristics of Na-A zeolites synthesized from Egyptian kaolinite for manganese in aqueous solutions: Response surface modeling and optimization. Applied Clay Science. 2017;140:17-24.

56. Sharifpour E, Khafri HZ, Ghaedi M, Asfaram A, Jannesar R. Isotherms and kinetic study of ultrasound-assisted adsorption of malachite green and Pb2+ ions from aqueous samples by copper sulfide nanorods loaded on activated carbon: Experimental design optimization. Ultrasonics Sonochemistry. 2018;40:373-82.

57. Asfaram A, Ghaedi M, Yousefi F, Dastkhoon M. Experimental design and modeling of ultrasound assisted simultaneous adsorption of cationic dyes onto ZnS: Mn-NPs-AC from binary mixture. Ultrasonics Sonochemistry. 2016;33:77-89.

58. Sepehr MN, Zarrabi M, Kazemian H, Amrane A, Yaghmaian K, Ghaffari HR. Removal of hardness agents, calcium and magnesium, by natural and alkaline modified pumice stones in single and binary systems. Applied Surface Science. 2013;274:295-305.

59. Yu Z, Qi T, Qu J, Wang L, Chu J. Removal of Ca(II) and Mg(II) from potassium chromate solution on Amberlite IRC 748 synthetic resin by ion exchange. Journal of Hazardous Materials. 2009;167(1-3):406-12.

60. Ramírez AM, Melo PG, Robles JMA, Castro MES, Khamkure S, León RGd. Kinetic and Thermodynamic Study of Arsenic (V) Adsorption on P and W Aluminum Functionalized Zeolites and Its Regeneration. Journal of Water Resource and Protection. 2013;05(08):58-67.

61. Khodadadi M, Malekpour A, Ansaritabar M. Removal

*J. Water Environ. Nanotechnol., 4(2): 119-138 Spring 2019*

137

of Pb (II) and Cu (II) from aqueous solutions by NaA zeolite coated magnetic nanoparticles and optimization of method using experimental design. Microporous and Mesoporous Materials. 2017;248:256-65.

62. Hadi N, Niaei A, Nabavi SR, Navaei Shirazi M, Alizadeh R. Effect of second metal on the selectivity of Mn/H-ZSM-5 catalyst in methanol to propylene process. Journal of Industrial and Engineering Chemistry. 2015;29:52-62.

63. Daud Z, Abu Bakar MH, Rosli MA, Ridzuan MB, Aliyu R. Application of response surface methodology (RSM) to optimize COD and ammoniacal nitrogen removal from leachate using moringa and zeolite mixtures. International Journal of Integrated Engineering. 2018;10(1).

64. Loiola AR, Andrade JCRA, Sasaki JM, da Silva LRD. Structural analysis of zeolite NaA synthesized by a cost-effective hydrothermal method using kaolin and its use as water softener. Journal of Colloid and Interface Science. 2012;367(1):34-9.

65. Bieseki L, Penha FG, Pergher SBC. Zeolite A synthesis employing a brazilian coal ash as the silicon and aluminum source and its applications in adsorption and pigment formulation. Materials Research. 2012;16(1):38-43.

66. Ghasemi Z, Younesi H. Preparation and Characterization of Nanozeolite NaA from Rice Husk at Room Temperature without Organic Additives. Journal of Nanomaterials. 2011;2011:1-8.

138

*J. Water Environ. Nanotechnol., 4(2): 119-138 Spring 2019*